Original Article

The role and mechanism of PDZ binding kinase in hypobaric and hypoxic acute lung injury

Linao Sun[1,2#], Haoran Yue[1,2#], Hao Fang[1,2#], Runze Li[1,2], Shicong Li[2], Jianyao Wang[1,2], Pengjie Tu[1,2], Fei Meng[1,2], Wang Yan[1,2], Jinxia Zhang[3], Elena Bignami[4], Kyeongman Jeon[5], Biniam Kidane[6], Peng Zhang[2]

[1]Graduate College of Tianjin Medical University, Tianjin, China; [2]Department of Cardiothoracic Surgery, Tianjin Medical University General Hospital, Tianjin, China; [3]Xianrenchang (Tianjin) Medical Technology Co., Ltd., Tianjin, China; [4]Anesthesiology, Critical Care and Pain Medicine Division, Department of Medicine and Surgery, University of Parma, Parma, Italy; [5]Division of Pulmonary and Critical Care Medicine, Department of Medicine, Samsung Medical Center, Sungkyunkwan University School of Medicine, Seoul, South Korea; [6]Section of Thoracic Surgery, University of Manitoba, Winnipeg, MB, Canada

Contributions: (I) Conception and design: L Sun, P Zhang; (II) Administrative support: P Zhang; (III) Provision of study materials or patients: P Zhang; (IV) Collection and assembly of data: L Sun, H Yue, H Fang; (V) Data analysis and interpretation: L Sun, H Yue, H Fang; (VI) Manuscript writing: All authors; (VII) Final approval of manuscript: All authors.

[#]These authors contributed equally to this work as co-first authors.

Correspondence to: Peng Zhang, BA. Department of Cardiothoracic Surgery, Tianjin Medical University General Hospital, 154 Anshan Road, Heping District, Tianjin 300052, China. Email: zhangpengtjgh@126.com.

Background: Acute lung injury (ALI) caused by hypobaric hypoxia (HH) is frequently observed in high-altitude areas, and it is one of the leading causes of death in high-altitude-related diseases due to its rapid onset and progression. However, the pathogenesis of HH-related ALI (HHALI) remains unclear, and effective treatment approaches are currently lacking.

Methods: A new mouse model of HHALI developed by our laboratory was used as the study subject (Chinese patent No. ZL 2021 1 1517241 X). Real-time quantitative polymerase chain reaction (RT-qPCR) was used to detect the messenger RNA (mRNA) expression levels of PDZ-binding kinase (*PBK*), sirtuin 1 (*SIRT1*), and PTEN-induced kinase 1 (*PINK1*) in mouse lung tissue. Hematoxylin and eosin staining was used to observe the main types of damage and damaged cells in lung tissue, and the lung injury score was used for quantification. The wet-dry (W/D) ratio was used to measure lung water content. Enzyme-linked immunosorbent assay was used to detect changes in inflammatory factors and oxidative stress markers in the lungs. Western blotting verified the expression of various mitochondrial autophagy-related proteins. The 5,5',6,6'-tetrachloro-1,1',3,3'-tetraethylbenzimi-dazoylcarbocyanine iodide (JC-1) method was used determined the health status of mitochondria based on changes in mitochondrial membrane potential. Transmission electron microscopy was used to directly observe the morphology of mitochondria. Multicolor immunofluorescence was used to observe the levels of mitochondrial autophagy markers. Other signaling pathways and molecular mechanisms that may play a role in epithelial cells were analyzed via through RNA sequencing.

Results: Low pressure and hypoxia caused pathological changes in mouse lung tissue, mainly ALI, leading to increased levels of inflammatory factors and intensified oxidative stress response in the lungs. Overexpression of *PBK* was found to alleviate HHALI, and activation of the *p53* protein was shown to abrogate this therapeutic effect, while activation of *SIRT1* protein reactivated this therapeutic effect. The therapeutic effect of *PBK* on HHALI is achieved via the activation of mitochondrial autophagy. Finally, RNA sequencing demonstrated that besides mitochondrial autophagy, *PBK* also exerts other functions in HHALI.

Conclusions: Overexpression of *PBK* inhibits the expression of p53 and activates *SIRT1-PINK1* axis mediated mitochondrial autophagy to alleviate HHALI.

Introduction

With the growing prevalence of acute lung injury (ALI) caused by hypobaric hypoxia (HH), clinical physicians are facing a significant challenge in treatment (1). In low-pressure atmospheres, such as at high altitudes, a decrease in oxygen partial pressure leads to reduced tissue oxygenation and triggers HH-related physiological responses (2). At the microscopic level, inadequate oxygen supply disrupts normal mitochondrial metabolism and imposes stress on biological systems (3). Mountaineers climbing at extreme altitudes may experience acute mountain sickness, severe hypoxia, and high-altitude cerebral edema, which can be life-threatening (4). In both humans and animal models, exposure to HH (>2,500 m) rapidly activates inflammatory processes (5,6). The pathological processes primarily induced by HH involve oxidative stress and inflammatory responses (7). The lungs, as the main organ for gas exchange and oxygen regulation, play a crucial role. Therefore, in hypoxic conditions, in addition to the brain, the lung is susceptible to damage and can

progress to ALI, especially injury to type II alveolar epithelial (ATII) cells (8-10). HH weakens the activity of mitochondrial energy synthesis complexes (complexes I, II, III, IV) and disrupt mitochondrial dynamics, impairing the cellular energy reservoir (11). Damaged mitochondria and excessive metabolic substrates can be removed through mitochondrial autophagy, which protects healthy mitochondria and prevents cascading reactions triggered by sustained oxidative stress caused by mitochondrial damage (12). HH induces molecular changes associated with oxidative stress, inflammation, and protein kinase activation (13).

PDZ-binding kinase (*PBK*), also known as T-lymphokine-activated killer cell-originated protein kinase (*TOPK*), is a serine/threonine kinase that participates in cell cycle regulation and mitotic progression (14,15). It is predominantly expressed in actively proliferating cells, particularly in hair follicle cells and embryonic cells (16,17). *PBK/TOPK* is primarily involved in the regulation of cell cycle and apoptotic pathways (17), and by phosphorylating its substrates to activate downstream signaling cascades, it plays significant roles in multiple cellular processes, including growth, development, cell apoptosis, and inflammation (16,17). *PBK/TOPK* also figures prominently in ischemic injury and is involved in ischemic protection and postischemic processing (18). Research suggests that the downregulation of *PBK* after paclitaxel treatment can enhance cell apoptosis, autophagy, and *p53* levels. *PBK* hinders paclitaxel-induced cell death by inhibiting *p53* (19). *PBK/TOPK* is also significantly involved in cell growth, DNA damage repair, immune response, and inflammation processes (20,21). At present, the treatment methods for HHALI are still very scarce. This study aims to explore a new treatment method, and *PBK* has been found to play a role in HHALI for the first time. However, the role of *PBK* in HHALI remains unclear, and thus the aim of this study was to examine the specific molecular mechanisms of *PBK* in HHALI. We present this article in accordance with the ARRIVE reporting checklist (available at https://jtd.amegroups.com/article/view/10.21037/jtd-24-188/rc).

Highlight box

Key findings
- For the first time, we report that PDZ-binding kinase (*PBK*) can serve as a potential therapeutic target for hypobaric and hypoxic acute lung injury (ALI).

What is known and what is new?
- In previous studies, PBK has been found to regulate the cycle and apoptosis of various tumor cells and to be involved in the occurrence and development of tumors.
- We investigated the molecular mechanisms by which *PBK* participates in normal lung epithelial cell apoptosis and its main signaling pathways, and demonstrated that PBK alleviates hypobaric and hypoxic ALI through mitochondrial autophagy.

What is the implication, and what should change now?
- PBK may be a potential therapeutic target for hypobaric and hypoxic ALI, providing a certain theoretical basis and guiding significance for high-altitude medical treatment.

2084

Sun et al. The role and mechanism of *PBK* in HHALI

Methods

Grouping of animal and cell models

Twenty-five Balb/c mice (male, 4 weeks, 20 g) were randomly divided into five groups (n=5; labeled group a, b, c, d, and e) via a random computer selection of animal numbers. Adenovirus transfection and the application of activators are all administered through nasal drops in mice. The groups were as follow: group a, adeno-associated virus serotype 5 (AAV5)-normal control (NC); group b, AAV5-NC + HH; group c, AAV5-*PBK* + HH; group d, AAV5-*PBK* + HH + *p53* activator (kevetrin hydrochloride); and group e, AAV5-*PBK* + HH + *p53* activator (kevetrin hydrochloride) + sirtuin 1 (*SIRT1*) activator (resveratrol). The Beas-2b cell line was also divided into five groups: group A, lentivirus (LV)-NC; group B, LV-NC + HH; group C, LV-*PBK* + HH; group D, LV-*PBK* + HH + *p53* activator (kevetrin hydrochloride); and group E, LV-*PBK* + HH + *p53* activator (kevetrin hydrochloride) + *SIRT1* activator (resveratrol). After the mice were anesthetized with phenobarbital, the lungs were extracted for subsequent experiments. The HH conditions for the animal and cell models were established using the hypobaric and hypoxic chamber developed by our laboratory. Balb/c mice were exposed to an extreme altitude of 8,500 m (33.1 kPa), while the Beas-2b cell line was exposed to an altitude of 6,500 m (44.0 kPa). The Beas-2b cell line was obtained from the Chinese Typical Culture Collection Center (Wuhan University Preservation Center), and Balb/c mice were purchased from Beijing Hualianke Biological Technology Co., Ltd, Beijing, China. The anesthetic use for all animal procedures in this study was propofol. All animal experiments were approved by the Animal Welfare and Ethics Committee of Tianjin Medical University General Hospital (No. IRB2023-DW-122), in compliance with national guidelines for the care and use of animals. A protocol was prepared before the study without registration.

Hematoxylin and eosin staining

Mouse lungs were fixed in paraffin and sliced into 4 µm sections. The sections were dried in an oven at 60 ℃ for 1–2 hours, which was followed by deparaffinization in xylene for 15 minutes. Subsequently, the sections were sequentially immersed in ethanol solutions of 100%, 95%, 75%, and 50% for 3 minutes each. After being rinsed with distilled water for 1 minute, the sections were stained with safranin. The sections were differentiated with a 1% hydrochloric acid ethanol solution, which was followed by a second rinse with a 0.2% ammonium hydroxide solution. After washing, the sections were stained with eosin and observed after being dried and mounted them in a fume hood.

Lung injury score

The degree of lung injury was assessed using a semiquantitative method. Each slice was scored by two pathology experts, with five different perspectives being observed for each slice. The severity of lung injury was classified into five levels: 0 (normal) to 4 (severe). Specifically, the pathological indicators included the degree of inflammatory cell infiltration, the degree of lung tissue congestion and hemorrhage, the degree of pulmonary edema, the degree of thickening of alveolar walls, and the formation of pulmonary hyaline membranes (22).

Real-time fluorescence quantitative polymerase chain reaction

The total RNA from and cells was extracted using TRIzol and reverse transcribed into complement DNA (cDNA) with 1 µg of RNA. The experiment was conducted using a 25 µL reaction system, including 12.5 µL of 2× Talent quantitative polymerase chain reaction (qPCR) premix, 1 µL of forward primer (10 mM), 1 µL of reverse primer (10 mM), 1 µL of cDNA, and 9.5 µL of RNase-free double-distilled water (ddH$_2$O). The primer sequence is provided in *Table 1*.

Flow cytometry

An Annexin V-fluorescein isothiocyanate (FITC)/propidium iodide (PI) cell apoptosis detection kit (Solarbio, Beijing, China) was used to detect cell cycle and apoptosis. The adherent cells were digested with 0.25% trypsin, centrifuged at 9.7 ×g for 5 minutes, and resuspended in precooled 1× phosphate-buffered saline (PBS). After centrifugation at 1,000 rpm for 5 minutes, the cells were resuspended in 300 µL of 1× binding buffer. After adding 5 µL of annexin V-FITC to cells, it was incubated at room temperature for 20 minutes in the dark. Flow cytometry was conducted for 5 minutes after PI was added.

Western blotting

After cells were lysed with protein lysis buffer, total protein

Table 1 Messenger RNA primer sequence

Target gene	Orientation	Primer sequence (5'-3')
β-actin (mouse)	Forward	AAGACCTCTATGCCAACACAG
	Reverse	GGAGGAGCAATGATCTTGATC
PBK (mouse)	Forward	TTGCTATGGAGTATGGAGGTG
	Reverse	GATACTTTAGCCCTCTTGCCA
SIRT1 (mouse)	Forward	CACTGTTGGTTGACTTCATCTTCC
	Reverse	CGGTGCTGACTCCTCACATT
PINK1 (mouse)	Forward	TATCTCGGCAGGTTCCTCCA
	Reverse	CGGACTTGAGATCCCGATGG
GAPDH (human)	Forward	GGAGCGAGATCCCTCCAAAAT
	Reverse	GGCTGTTGTCATACTTCTCATGG
PBK (human)	Forward	ATCCCGGCCTCTCCGTTTAT
	Reverse	GTTATGAAGGCAGGAGCAGTC
PINK1 (human)	Forward	TTGCCCCTAACACGAGGAAC
	Reverse	ACGTGCTGACCCATGTTGAT
SIRT1 (human)	Forward	CTACTGGCCTGAGGTTGAGG
	Reverse	GGACGGAGGAAAAGAGCGAA

RNA, ribonucleic acid; *PBK*, PDZ binding kinase; *SIRT1*, Sirtuin 1; *PINK1*, PTEN induced kinase 1; *GAPDH*, glyceraldehyde-3-phosphate dehydrogenase.

was extracted, and the protein concentration was determined using the bicinchoninic acid (BCA) method. The total protein amount was calculated, and 20 μg protein samples were loaded. The protein samples (20 μg) were separated by electrophoresis and transferred onto a membrane. After the membrane was blocked at room temperature for 2 hours, it was incubated overnight at 4 ℃ with primary antibodies against *PBK*, *SIRT1*, PTEN-induced kinase 1 (*PINK1*), *p53*, *parkin*, *caspase3*, *BCL2* apoptosis regulator (*BCL2*), *BCL2*-associated X, apoptosis regulator (*BAX*), and *GAPDH*. Subsequently, the membrane was incubated at room temperature with secondary antibodies (anti-rabbit or anti-mouse; 1:2,000) for 2 hours, which was followed by enhanced chemiluminescence detection and protein expression analysis using ImageJ software (US National Institutes of Health).

Enzyme-linked immunosorbent assay

The optical density (OD) values of interleukin 1β (IL-1β), tumor necrosis factor α (TNF-α), total-superoxide dismutase (T-SOD), and malondialdehyde (MDA) were measured at 450 nm using an enzyme-linked immunosorbent assay (ELISA) reader according to the instructions of the kit (Bioss, Beijing, China). A standard curve was plotted for the samples, and the concentrations were calculated.

5,5',6,6'-tetrachloro-1,1',3,3'-tetraethylbenzimidazoylcarbocyanine iodide (JC-1) mitochondrial membrane potential detection

After the cells were incubated with JC-1 staining solution (Beyotime) for 20 minutes, the changes in mitochondrial membrane potential in cells were evaluated by measuring the fluorescence intensity under laser confocal microscopy. The wavelength of J monomers was 495/519 nm, while the wavelength of J aggregates was 550/570 nm. Quantitative measurements were performed using ImageJ software.

Observation of mitochondrial morphology under transmission electron microscopy

After the five sets of cell samples were rinsed with sterile PBS solution two or three times, the cells were placed in a sterile centrifuge tube as longitudinal sections with a cross-sectional area of about 1 mm^3 and a length of a strip, after which precooled 2% glutaraldehyde fixative solution was added. The electron microscope samples were fixed in a 1% osmium tetroxide solution for 2 hours, dehydrated with a gradient of ethanol and acetone, embedded in epoxy resin, and polymerized in a 65 ℃ oven for 48 hours. Following this, the samples were sectioned into semithin slices, and specific regions were selected for observation under a transmission electron microscope.

Wet-dry ratio

The right lung lobe of mice was extracted, and its weight was measured using a precision balance, with the result being recorded as the wet lung weight. The wet lung was placed in a container and air-dried at 60 ℃ in an oven for 72 hours. Subsequently, the lung weight was measured as the dry lung weight. The wet-dry (W/D) ratio was calculated by dividing the wet lung weight by dry lung weight.

Multicolor immunofluorescence

When the Beas-2b cell line was cultured to 70% of the culture dish, 95% alcohol was used to fix the cells. After

triton was used to penetrate the cell membrane, the first antibody (*LC3B*, *TOMM20*) was incubated overnight at 4 ℃, and the second antibody (Rabbit anti sheep) was stained with fluorescent dye and incubated for 2 hours. After thorough washing, the above steps were repeated, and the fluorescence excitation of the corresponding dye was observed.

Differential gene and pathway enrichment analysis

Differential analysis was conducted based on transcriptome sequencing data between the LV-NC group and the LV-*PBK* group to identify differentially expressed genes [$\log_2$ fold change (FC) =1 and P=0.05], and duplicate genes were normalized. The functions of different genes in the two groups were analyzed using Gene Ontology (GO) and Kyoto Encyclopedia of Genes and Genomes (KEGG). Pathway enrichment was analyzed using gene set enrichment analysis (GSEA) [false discovery rate (FDR) <0.25, adjusted P value <0.05], with the selected annotated gene set files being "h.all.v2023.1.Hs.symbols.gmt" (specifically defined biological states or processes), "c3.all.v2023.1.Hs.symbols.gmt" (microRNA and transcription factor features), and "c7.all.v7.4.symbols.gmt" (immunological features).

Statistical analysis

Bioinformatics analysis was performed using version the R software version 4.2.1 (www.r-project.org). Correlation analysis, differential analysis, and functional enrichment analysis were conducted using the "psych", "DESeq2", "enrichplot", and "clusterProfilter" packages in R. GSEA was performed using GSEA software version 4.3.2 e (www.gsea-msigdb.org/gsea). Data analysis was conducted using statistical SPSS 26.0 (IBM Corp.), ImageJ, and GraphPad Prism 8 (GraphPad Software). The data are presented as the mean ± standard deviation. After the homogeneity of variance was tested, intergroup comparisons were performed using one-way analysis of variance. The level of statistical significance was set at P<0.05.

Results

The type of injuries in bronchial epithelial cells and Balb/c mouse lungs exposed to HH

After HH exposure, pathological changes in mouse lungs mainly included inflammatory cell infiltration, pulmonary congestion, interstitial edema, thickening of alveolar walls,

and continuous interruption of alveoli, indicating ALI (*Figure 1A*). Lung injury scores were evaluated using the aforementioned method, and the lung injury score of the HH group was significantly higher than that of the control group (*Figure 1B*), indicating that mouse lungs undergo a certain degree of acute pathological changes after exposure to HH for 4 days. The W/D ratio in lung increased, indicating an increase in the degree of pulmonary edema (*Figure 1C*). Flow cytometry results showed an increase in cell apoptosis of Beas-2b under HH. Secretion of inflammatory factors (TNF-α and IL-1β) increased in injured lungs (*Figure 1D-1G*). Under exposure to an altitude of 6,500 m, the expression levels of *PBK* and *PINK1* mRNA in Beas-2b decreased, while the expression level of *SIRT1* mRNA did not show significant changes. The expression level of *PBK* mRNA in mouse lungs also decreased (*Figure 1H-1K*).

Construction of the PBK-overexpressing Beas-2b and Balb/c mouse model

Adenovirus-specific over-expression of *PBK* was conducted in mouse lungs, leading to elevated expression levels of *PBK* mRNA and protein in the lung (*Figure 2A-2C*). The stable cell line was obtained by transfecting Beas-2b with lentivirus, resulting in an increased expression level of *PBK* mRNA (*Figure 2D,2E*) and a corresponding increase in the relative expression level of the protein (*Figure 2F*).

Overexpression of PBK alleviated pulmonary edema and mitigated HHALI

After construction of the *PBK*-overexpressing Beas-2b and Balb/c mouse models, the therapeutic effect of *PBK* also manifested macroscopically in mouse lungs. The reduction of inflammatory areas in the lungs of *PBK*-overexpressing mice was clearly visible and was accompanied by vasodilation and alleviation of pulmonary congestion symptoms. This effect was also abolished by *p53* agonists and was reversed by *SIRT1* agonists (*Figure 3A*). As observed by hematoxylin and eosin (HE) staining of lung tissue pathological sections, the lungs in the HH group and *p53* agonist group showed inflammatory cell infiltration, red blood cell extravasation, interstitial edema, thickening of alveolar walls, and discontinuity of alveoli, while the lung injury scores in the group c and group e were significantly lower than those in the group b and group d (*Figure 3B,3C*). In terms of the degree of pulmonary edema, the lung water content in the group c and group e was lower than that in
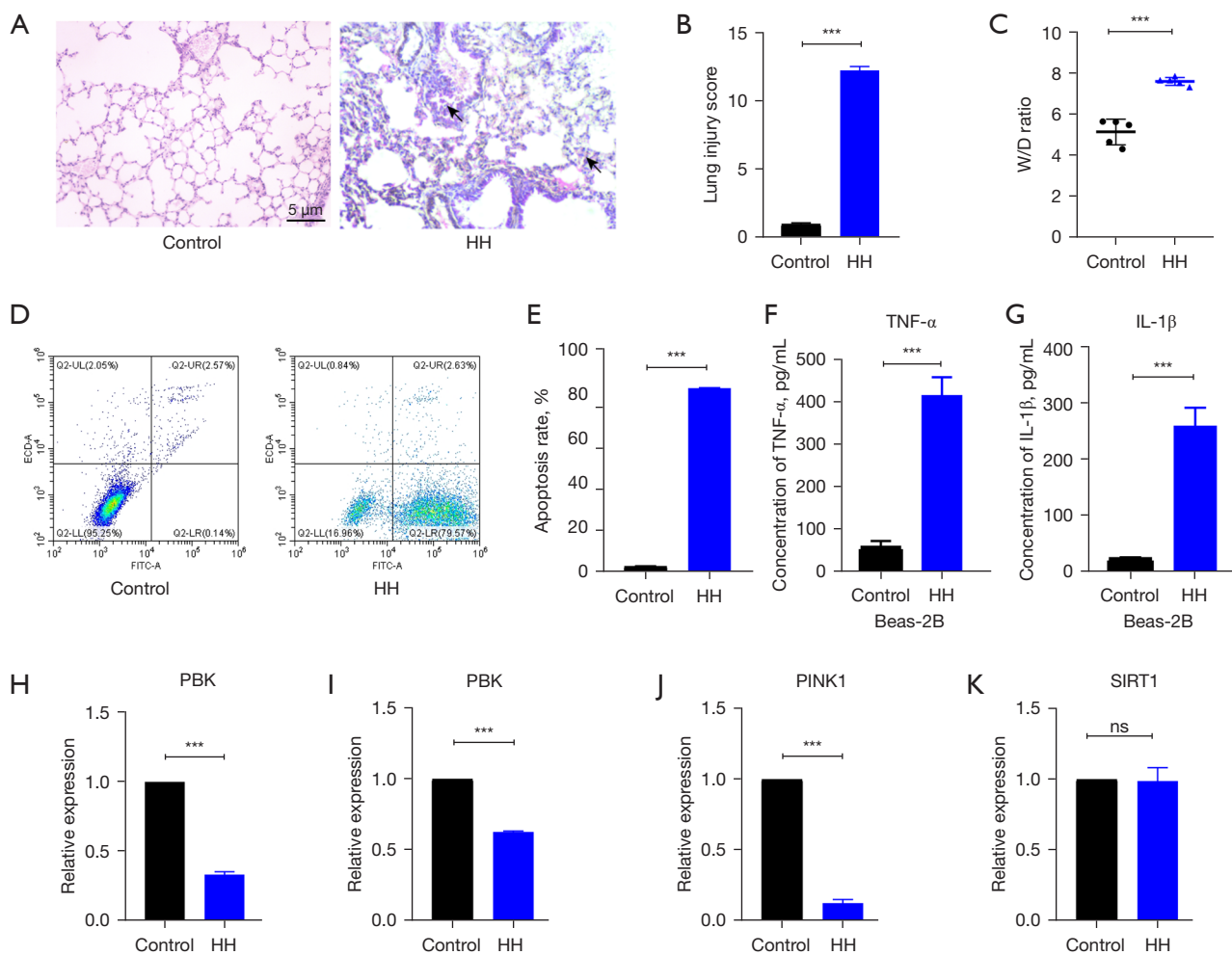
Figure 1 Pathological and genetic changes in cells and mice in an HH environment. (A-C) HE staining (×200) of lungs in HH mice (n=3) and control mice (n=3), lung injury score, and W/D ratio, the black arrow represents the obvious damage area. (D,E) Apoptosis level in Beas-2b cells. (F,G) Levels of inflammatory factors (TNF-α and IL-1β) in Beas-2b cells. (H) Relative mRNA expression levels of *PBK* in HH mice (n=5) and control mice (n=5). (I-K) Relative mRNA expression levels of *PBK*, *PINK1*, and *SIRT1* in the HH group and control group of Beas-2b cells. ***, P<0.001; ns, no significance. HH, hypobaric-hypoxic; W/D ratio, wet-dry ratio; TNF-α, tumor necrosis factor alpha; IL-1β, interleukin 1 beta; *PBK*, PDZ binding kinase; *SIRT1*, Sirtuin 1; *PINK1*, PTEN induced kinase 1; PTEN, mutated in multiple advanced cancers 1.

the group b and group d (*Figure 3D*).

Upregulation of PBK reduced cell apoptosis

We found that the overexpression of *PBK* significantly reduced the apoptosis rate of Beas-2b cells exposed to HH (*Figure 4A,4B*). This therapeutic effect was abolished by the *p53* agonist, but reappeared after *SIRT1* was reactivated. The apoptosis levels of the group C and the group E were significantly alleviated compared to the group B and the

group D (*Figure 4C-4F*), indicating a pronounced mitigation of apoptosis-related protein expression in mouse lungs.

Overexpression of PBK reduced the secretion of inflammatory factors in the lungs and lowered the oxidative stress levels

Under HH conditions, the levels of inflammatory factors (IL-1β and TNF-α) in mouse lungs significantly increased (*Figure 5A,5B*). There was also an increase in the levels of
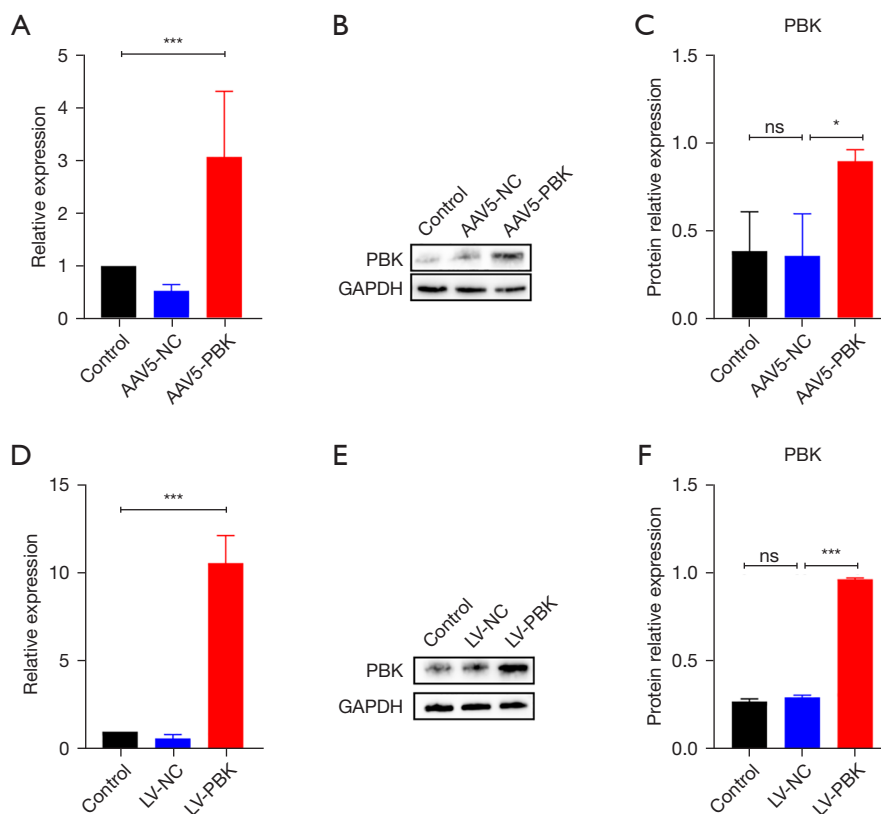
Figure 2 Construction of *PBK*-overexpression models in mice and cells. (A-C) Relative expression levels of *PBK* mRNA and protein in the lung tissue of Balb/c mice after nasal transfection with empty adenovirus AAV5-NC and *PBK* over-expressing adenovirus AAV5-*PBK*. (D-F) *PBK* mRNA and protein expression levels in Beas-2b cells after stable transfection with empty lentivirus LV-NC and *PBK* over-expressing lentivirus. *, P<0.05; ***, P<0.001; ns, no significance. *PBK*, PDZ binding kinase; AAV, adenovirus; LV, lentivirus; NC, normal control.

metabolic products of peroxides (MDA) and a decrease in the levels of antioxidant stress enzymes (T-SOD) (*Figure 5C,5D*). The activation of *p53* protein counteracted the therapeutic effect of *PBK*, while the activation of both *p53* and *SIRT1* reconstituted the alleviating effect of *PBK*.

Overexpression of PBK improved mitochondrial health in the Beas-2b cells exposed to HH

The activity and health of mitochondria were detected using the JC-1 method. The process of conversion from red fluorescence to green fluorescence indicated a gradual decrease in mitochondrial health. Exposure to HH reduced the health of cellular mitochondria, while overexpression of *PBK* exerted a certain degree of protection for mitochondria. The protective effect of *PBK* on mitochondria was inhibited by *p53*, whereas *SIRT1* had the opposite effect (*Figure 6A,6B*). The health of mitochondria was evaluated based on the

ratio of average fluorescence intensity between red and green fluorescence, with a lower ratio indicating better mitochondrial health and better activity, and vice versa.

Overexpression of PBK promoted mitochondrial autophagy and maintained normal mitochondrial morphology in Beas-2b cells

The multicolor immunofluorescence technique was employed to observe the expression levels of microtubule-associated protein 1 light chain 3 beta (*LC3B*) in cells. Translocase of outer mitochondrial membrane 20 (*TOMM20*) was labeled with brown fluorescence to indicate the position of mitochondria. Blue fluorescence indicated 4,6-diamino-2-phenyl indole (DAPI), and red fluorescence indicated *LC3B*. After exposure to HH, the fluorescence intensity of *LC3B* in cells decreased significantly. In groups C and E, the fluorescence intensity of *LC3B* was
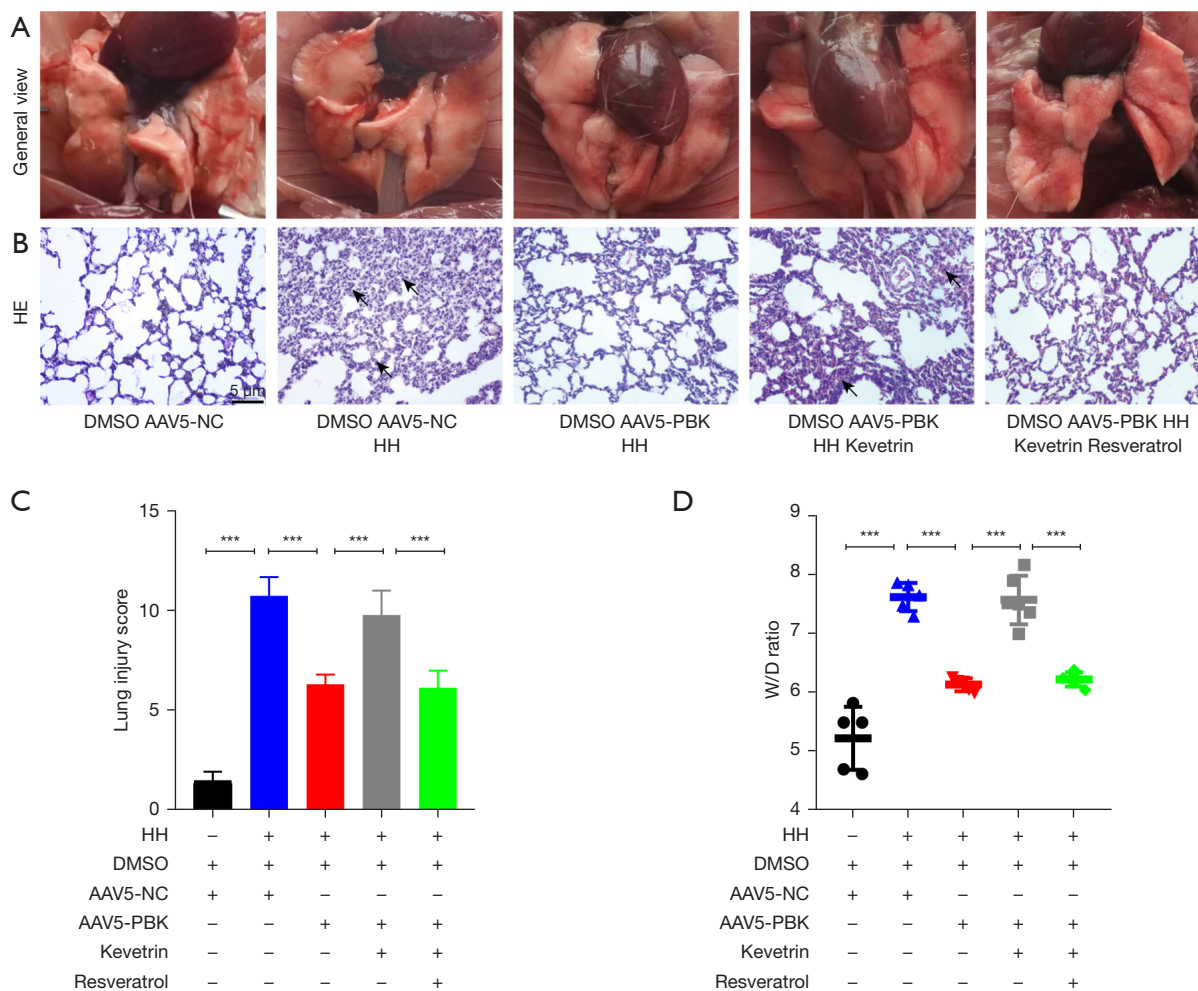
Figure 3 The regulatory effect of *PBK* on pulmonary pathological changes in mice. (A) Macroscopic observations of dissected lungs from Balb/c mice; (B-D) lung injury scoring, and W/D ratio of Balb/c mice, the black arrow represents the obvious damage area (HE, ×200). ***, P<0.001. *PBK*, PDZ binding kinase; W/D ratio, wet-dry ratio; AAV, adenovirus; HH, hypobaric hypoxia; NC, normal control.

significantly higher than that in groups B and D (*Figure 7A,7B*). We observed that the morphology of mitochondria tended to be normal in groups C and E, whereas in groups B and D, mitochondria exhibited enlargement, swelling, disordered cristae, and unclear matrix aggregation. Additionally, a positive correlation was observed between the quantity of autophagosomes in the cytoplasm and the proportion of healthy mitochondria. This suggests that autophagosomes are capable of identifying and engulfing dysfunctional mitochondria (*Figure 7C*).

Expression levels of proteins associated with mitochondrial autophagy

The fluorescence staining of mitophagy-related proteins

(*parkin*, *SIRT1*, and *PINK1*) showed a similar trend to that of *LC3B*. This suggested that the overexpression of *PBK* can activate mitophagy in Beas-2b cells, with this effect being achieved through the *p53-SIRT1-PINK1* axis (*Figure 8A-8F*).

Analysis of differential genes and protein interactions

We performed differential gene analysis between the LV-NC group and the LV-*PBK* group, and 510 differentially expressed genes were identified ($|\log_2 FC| > 1$ and P<0.05; *Figure 9A*). We selected the top 57 differentially expressed genes based on $|\log_2 FC|$ to generate a heatmap (*Figure 9B*). We conducted protein interaction analysis of the differentially expressed genes with $|\log_2 FC| > 4$ using the Search Tool for the Retrieval of Interacting Genes/Proteins
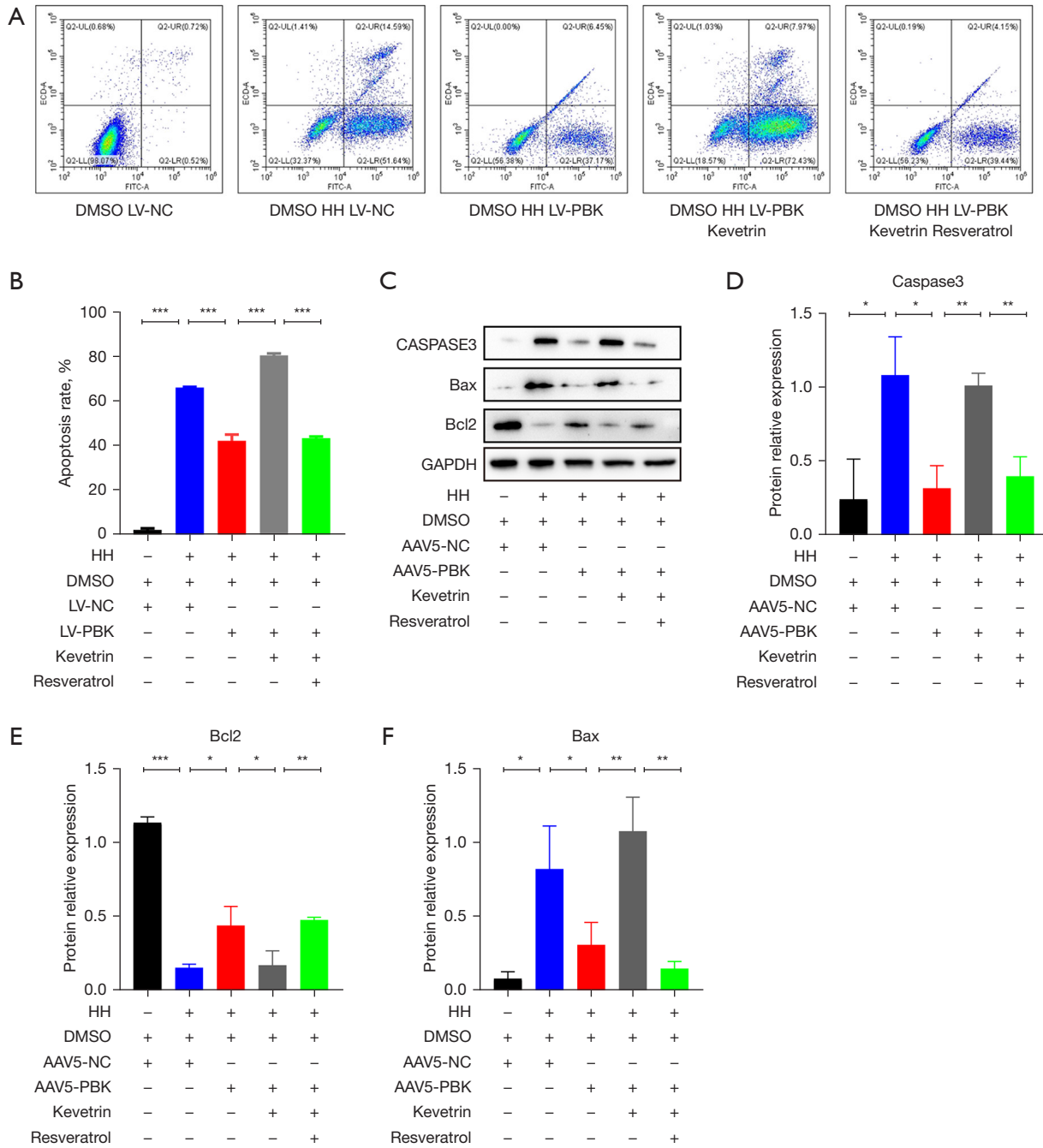
2090

Sun et al. The role and mechanism of *PBK* in HHALI

Figure 4 The role and mechanism of *PBK* in the apoptosis of mice and cells. (A,B) The apoptosis rate of the five groups of Beas-2b cells; (C-F) expression levels of apoptosis-related proteins caspase 3, *Bax*, and *Bcl2* in the five groups of Balb/c mouse lungs. *, P<0.05; **, P<0.01; ***, P<0.001. *PBK*, PDZ binding kinase; *Bax*, *BCL2* associated X, apoptosis regulator; *Bcl2*, *BCL2* apoptosis regulator; AAV, adenovirus; LV, lentivirus; NC, normal control; HH, hypobaric hypoxia.

(STRING) database (https://cn.string-db.org/) to observe the interactions between them. *Figure 9C* shows the proteins with connections. To investigate whether *PBK* plays a

role in other pathways, we conducted correlation analysis between *PBK* and key proteins in nine classic pathways, including NF-κB. *PBK* was significantly correlated with
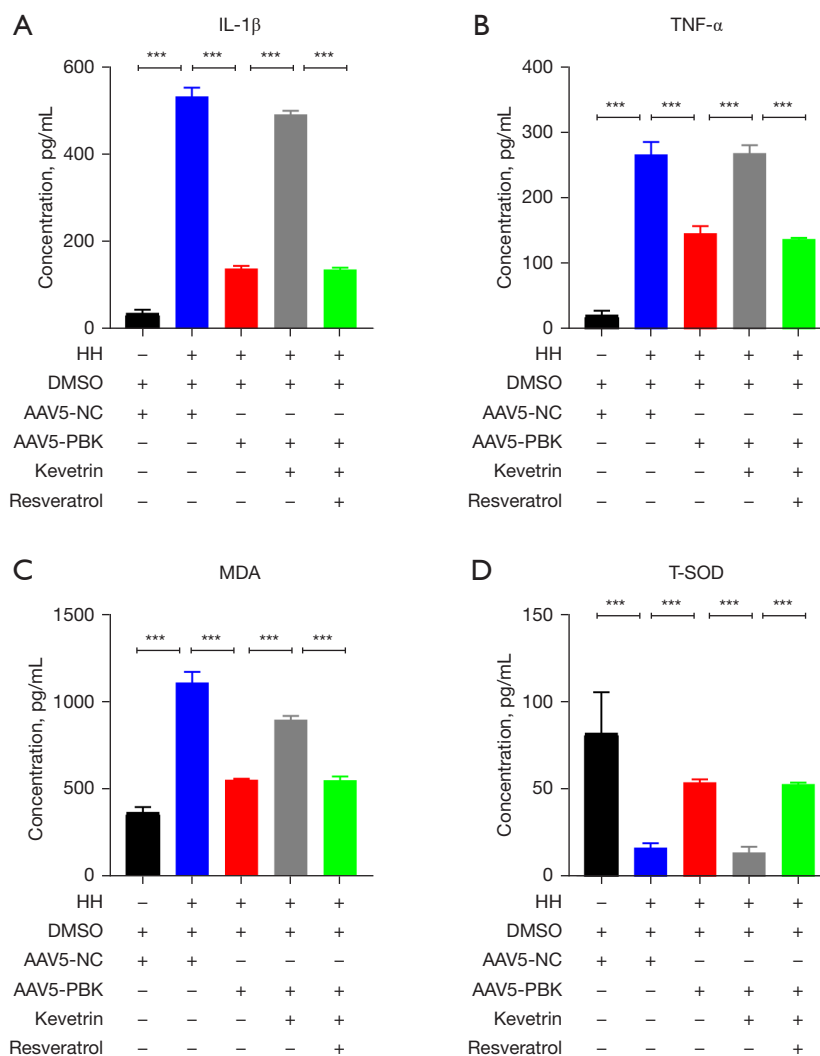
Figure 5 The regulatory effect of *PBK* on inflammatory factors and oxidative stress response. (A,B) Concentrations of IL-1β and TNF-α in the serum of Balb/c mice. (C,D) Concentrations of MDA and T-SOD in the Balb/c mouse lung homogenates. ***, P<0.001. *PBK*, PDZ binding kinase; TNF-α, tumor necrosis factor alpha; IL-1β, interleukin 1 beta; MDA, malondialdehyde; T-SOD, total-superoxide dismutase; AAV, adenovirus; HH, hypobaric hypoxia; NC, normal control.

PI3K/AKT, Wnt, and TGF-β, and other classic signaling pathways (*Figure 9D*).

Functional enrichment analysis

GO and KEGG enrichment analysis revealed functional differences between the LV-NC group and the LV-*PBK* group. The GO clustering plot displayed the top five enriched terms, including defense response to viruses, defense response to symbionts, response to viruses, leukocyte chemotaxis, and cell chemotaxis (*Figure 10A*).

In the categories of biological processes (BP), cellular components (CC), and molecular functions (MF), the top 10 enriched results included signal receptor agonists, collagen-containing extracellular matrix, and positive regulation of cytokine production (*Figure 10B*). In the KEGG enrichment analysis, top five most enriched pathways included TNF signaling pathway, IL-17 signaling pathway, rheumatoid arthritis, Epstein-Barr viral infection, and the interaction between viral proteins and cytokines and cytokine receptors (*Figure 10C*). The bubble chart in *Figure 10D* displays the top 35 most enriched pathways.

J Thorac Dis 2024;16(3):2082-2101 | https://dx.doi.org/10.21037/jtd-24-188

2092
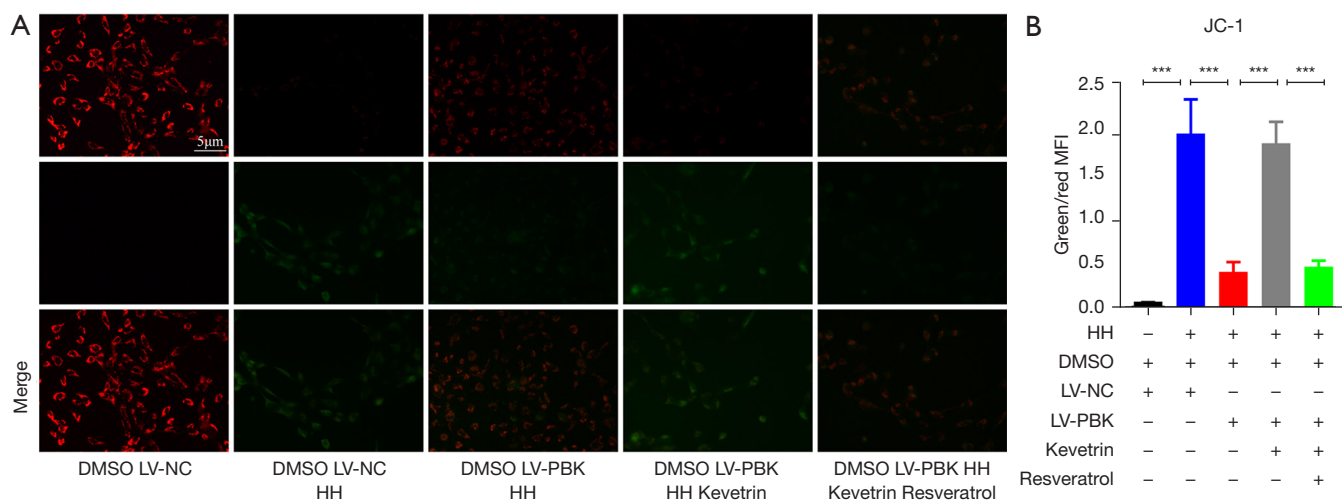
Sun et al. The role and mechanism of *PBK* in HHALI

Figure 6 The effect and mechanism of *PBK* on mitochondrial activity. (A,B) Red and green fluorescence staining was used to assess the mitochondrial membrane potential in Beas-2b cells. Red fluorescence represented JC-1 aggregates, while green fluorescence represented JC-1 monomers. The average fluorescence intensity was calculated, and statistical analysis was performed based on the green-red fluorescence ratio. ***, P<0.001. *PBK*, PDZ binding kinase; JC-1, 5,5',6,6'-tetrachloro-1,1',3,3'-tetraethyl-imidacarbocyanine; LV, lentivirus; NC, normal control; HH, hypobaric hypoxia; MFI, mean fluorescence intensity.

Different gene sets were selected for GSEA to identify the pathways of the LV-*PBK* group (FDR <0.25 and adjusted P value <0.05). The GSEA enrichment plot in *Figure 10E* shows the top 10 most active pathways in the hallmark gene set, indicating significant enrichment of these pathways in the LV-*PBK* group, including for reactive oxygen species, epithelial–mesenchymal transition, inflammatory response, and oxidative phosphorylation. Enrichment analysis was also performed on the transcription factor, microRNA feature, and immune feature gene sets, with the top 10 most active pathways being presented in Figure S1A,S1B. The results of functional enrichment analysis revealed the potential mechanisms or key nodes involved in disease occurrence and development, which may further inform treatment and improve the prognosis of patients.

Discussion

ALI and acute respiratory distress syndrome are pulmonary diseases (23), characterized by acute onset, histological evidence of lung parenchymal injury, increased permeability of the alveolar–capillary barrier, development of inflammatory response (i.e., cytokine storm and neutrophil recruitment), and respiratory dysfunction characterized by decreased PaO_2 (24,25). ALI is typically associated with extensive airway inflammation, hypoxemia, tissue disruption, and a lack of effective treatment (26). Plateau areas account for a large proportion of China's land area, and it is not uncommon for many mountaineers to suffer from HHALI due to rapid mountaineering. There are diverse causes of ALI. Patients who develop ALI due to low-pressure and low-oxygen conditions typically have a history of exposure to high-altitude regions and may also have concurrent damage to other high-altitude organs, such as high-altitude cerebral edema. However, there is currently no good treatment for HHALI. We have found for the first time that *PBK* may play a therapeutic role in ALI caused by low pressure and hypoxia.

In this study, we used a newly developed HHALI Balb/c mouse model. For the first time, we simulated the extreme altitude of 8,500 m using an HH animal culture chamber. Under this pressure condition, the mouse lung tissue experienced acute injury within a short period of time (4 days). Exposed to extreme altitude, we observed pathological changes in mouse lung tissue, primarily characterized by pulmonary edema, pulmonary hemorrhage, alveolar septal rupture, and inflammatory cell infiltration. According to the literature, chronic injury was mainly characterized by thickening of the vascular intima, pulmonary hypertension, and interstitial thickening (26,27). Additionally, we compared the HHALI mouse models created in other studies (28,29). Combining these
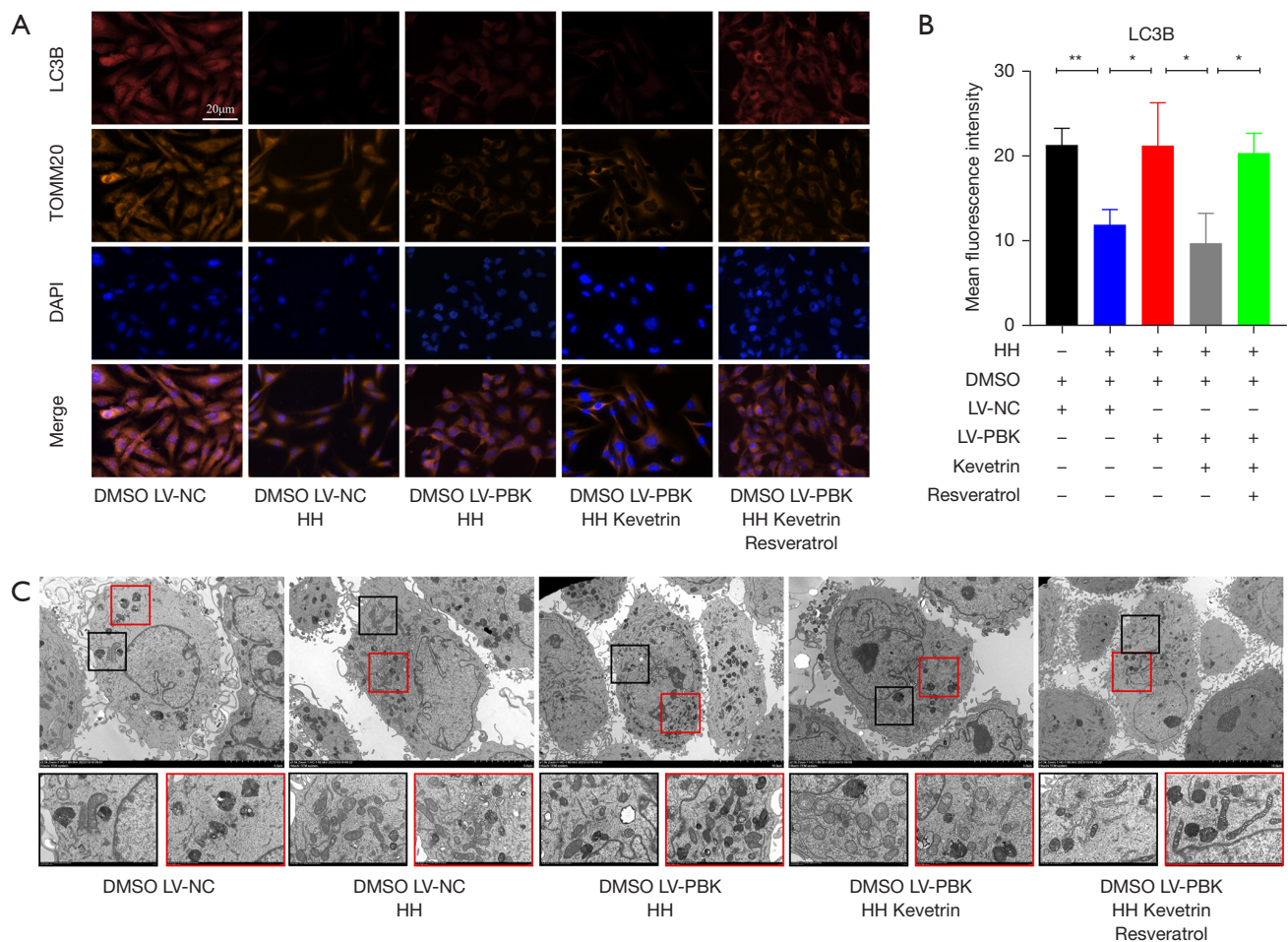
Figure 7 The effect and mechanism of *PBK* on mitochondrial the autophagy-related protein *LC3B* and mitochondrial morphology. (A,B) Multicolor immunofluorescence of Beas-2b cells was performed, with red fluorescence representing *LC3B* and brown fluorescence representing *TOMM20*. The average fluorescence intensity was calculated, and statistical analysis was conducted based on the green-red fluorescence ratio. (C) The microstructure of five cell groups was observed (Transmission electron microscope, ×10,000), with mitochondria morphology indicated by the black box (Transmission electron microscope, ×15,000), and autophagosomes indicated by the red box (Transmission electron microscope, ×15,000). *, $P<0.05$; **, $P<0.01$. *PBK*, PDZ binding kinase; *LC3B*, microtubule associated protein 1 light chain 3 beta; *TOMM20*, translocase of outer mitochondrial membrane 20; LV, lentivirus; NC, normal control; HH, hypobaric hypoxia.

observations with macroscopic examination, we can conclude that the model we established is ALI, not chronic lung injury. Flow cytometry results showed an increase in bronchial epithelial apoptosis rate and an elevation in the *Bcl2*-caspase 3 ratio in mouse lung tissue after 6 hours of exposure to HH conditions. Most researchers believe that apoptosis is a metabolically active process in which cell death occurs and exhibits characteristic morphological features, including cell membrane shrinkage, chromatin condensation, nuclear fragmentation, and membrane blebbing. In contrast, when cells undergo accidental death due to extreme or rapid injury, necrosis occurs, leading to plasma membrane dissolution, cell swelling, and release of intracellular contents that promote inflammation (30-32). Our flow cytometry experiments also indicated a significant increase in apoptosis in the lungs under HH. *PBK* expression decreased after exposure to HH. *PBK* is involved in cell cycle and apoptosis and regulates cell proliferation. Therefore, we believe that *PBK* has an indispensable role in cell apoptosis after exposure to HH. Our experiments also indirectly support the conclusions in the literature stating that the *SIRT1–PINK1* axis is critical to mitochondrial

2094

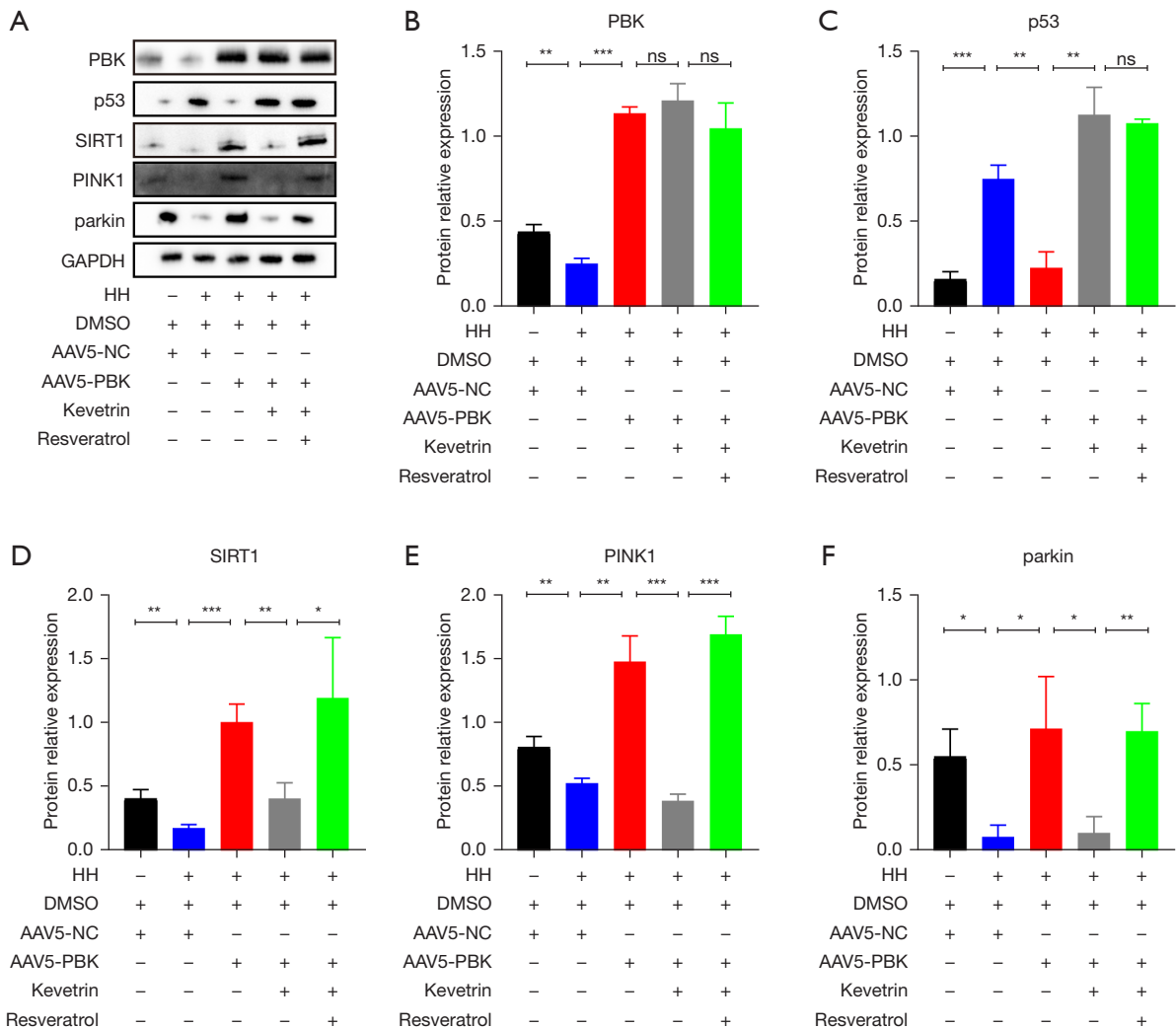Sun et al. The role and mechanism of *PBK* in HHALI

Figure 8 *PBK* affected the expression of downstream proteins and signaling molecules. Expression levels of *PBK*, *p53*, *SIRT1*, *PINK1*, and parkin proteins in the lungs of Balb/c mice. *, $P<0.05$; **, $P<0.01$; ***, $P<0.001$; ns, no significance. *PBK*, PDZ binding kinase; *SIRT1*, Sirtuin 1; *PINK1*, PTEN induced kinase 1; *PTEN*, mutated in multiple advanced cancers 1; AAV, adenovirus; NC, normal control; HH, hypobaric hypoxia.

autophagy (32,33). In our study, when *PBK* regulated *SIRT1*, there was no significant change in the transcription level of *SIRT1*, while the protein level significantly increased. This indicates that *PBK* regulates *SIRT1* by activating its protein activity.

During HHALI, inflammatory factors and oxidative stress markers generally increase in the lungs (34,35). Increased levels of inflammatory factors (IL-1β, TNF-α) in the serum indicate that the body is under stress. In a HH environment, the body triggers an immune response due to hypoxia. Inflammatory factors can only serve as markers for early

onset of hypoxia and cannot be used as criteria for assessing ALI. ALI occurred in mice exposed to low-pressure and low-oxygen conditions, with a rapid increase in inflammatory factors in the serum. Following PBK overexpression, there was a decline in inflammatory factors associated with the reduction of reactive oxygen species, indicating that inflammatory factors alone cannot be used as indicators of injury mitigation. In the mouse model used in our study, there was a similar upward trend observed for inflammatory factors and oxidative stress markers. Activation of inflammatory and oxidative stress responses occurred in mouse lung tissue
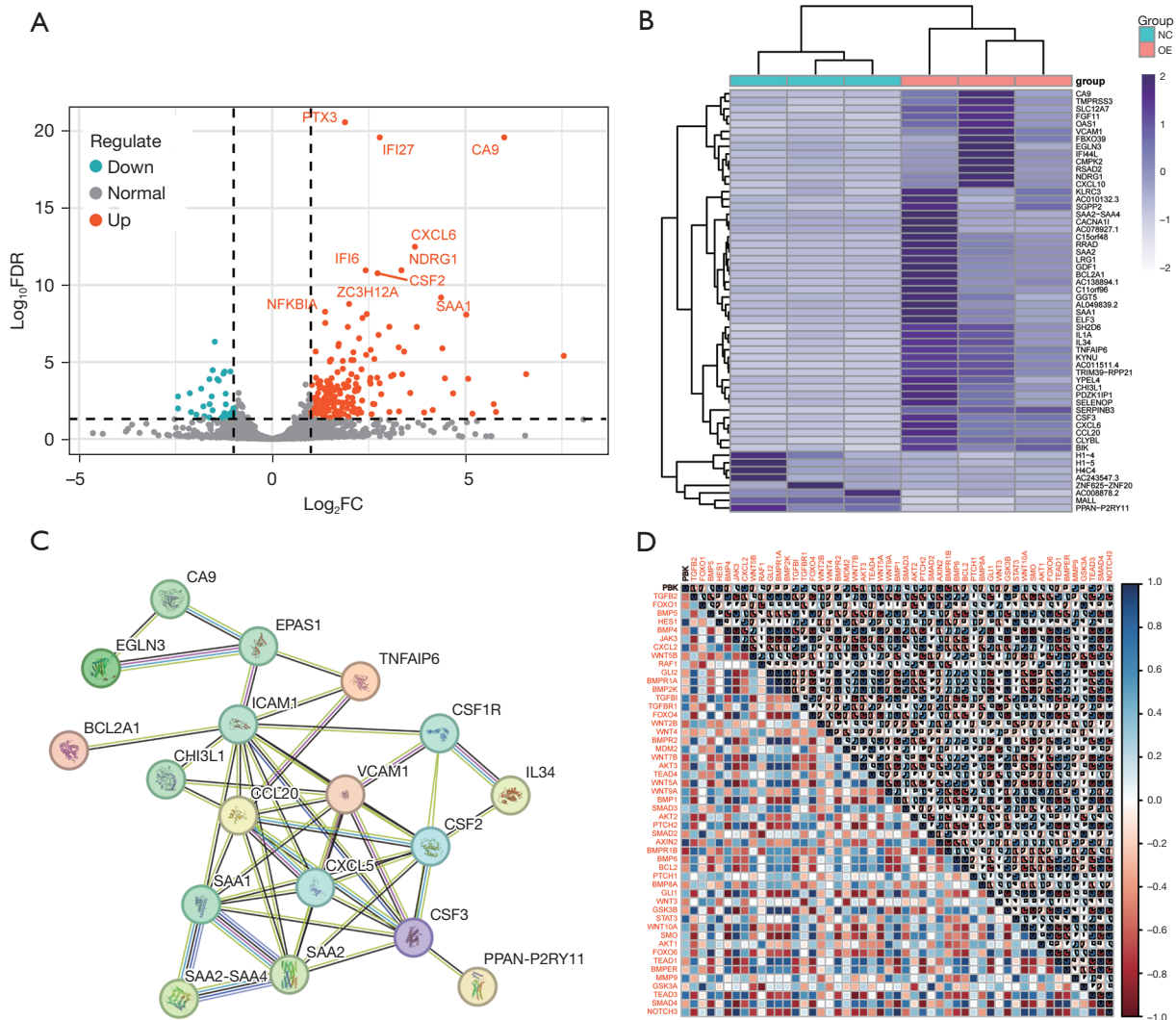
Figure 9 Analysis of other genes and signaling pathways that may interact with *PBK*. (A) Volcano plot of the differential genes between the LV-NC and LV-*PBK* groups. (B) Heatmap of the top 57 differential genes between the LV-NC and LV-*PBK* groups. (C) Protein interactions maps for the differential genes with |log₂FC| >4. (D) Correlation analysis of *PBK* with key proteins of nine classical signaling pathways. *PBK*, PDZ binding kinase; LV, lentivirus; NC, normal control; FDR, false discovery rate; FC, fold change.

under HH, which may be related to cell apoptosis (36,37). We speculate that inadequate oxygen supply for maintaining normal mitochondrial metabolism in HH environment results in oxidative stress reactions in mitochondria (38). This then leads to an increase in the generation of peroxides and superoxides (39), as well as a reduction in the synthesis of enzymes, such as peroxiredoxins, that mitigate oxidative stress reactions (40,41). As a result, the generated peroxides and superoxides are recognized as antigens by the body, initiating a vascular defense response against antigens and activating local inflammatory reactions. The

recruited inflammatory cells release a substantial amount of inflammatory factors, which subsequently damage normal cells in the region, resulting in increased apoptosis following cell injury (42). The ruptured cells further release a significant amount of peroxides, superoxides, and lysozyme substances, intensifying cell damage and establishing a vicious cycle (43), a cycle which was interrupted by *PBK* in our study. When cells are deprived of oxygen, mitochondria undergo oxidative stress. In this condition, upregulation of *PBK* can inhibit the transmission of the signaling molecule *p53*, leading to the activation of the downstream SIRT–
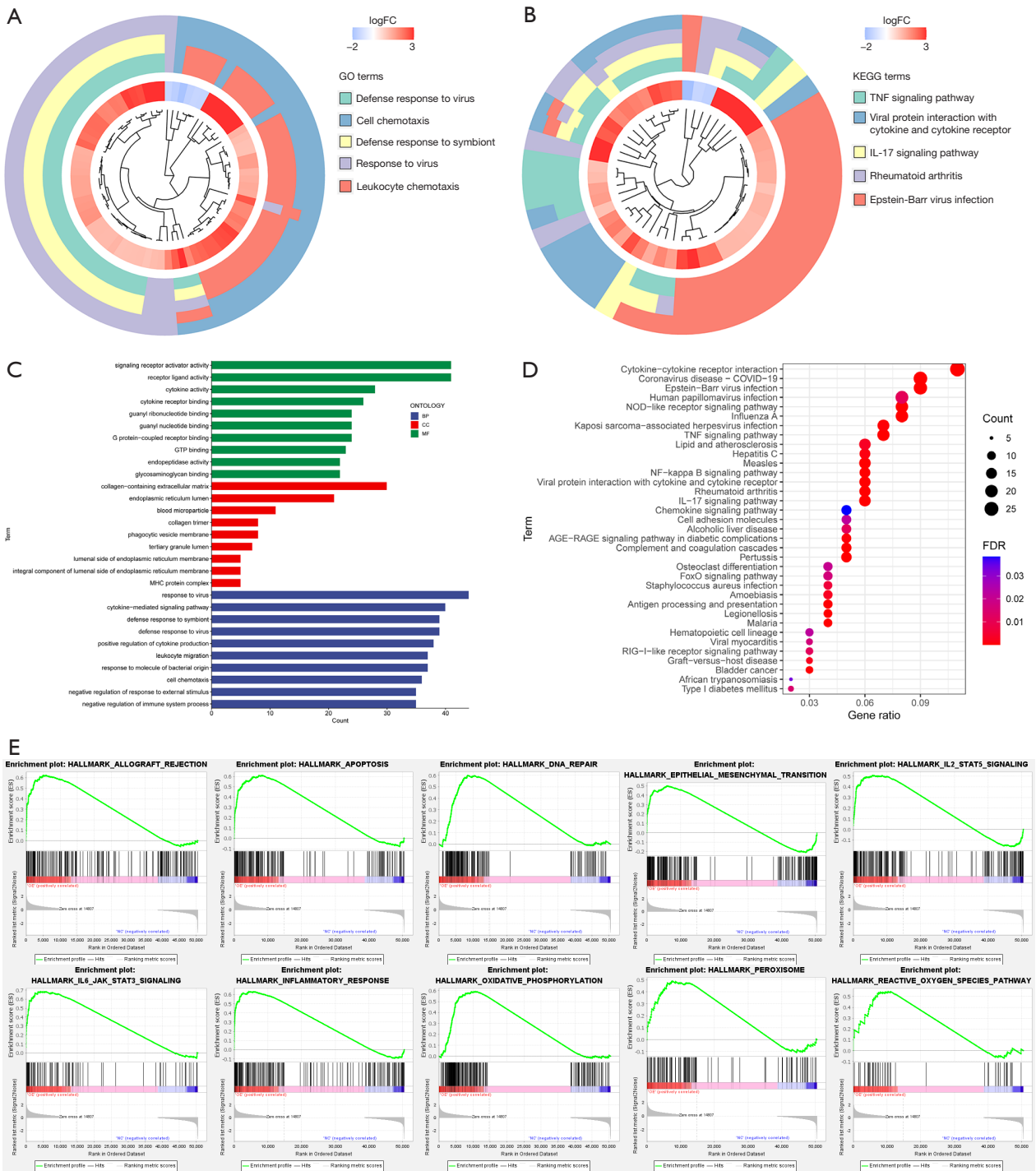
2096

Sun et al. The role and mechanism of *PBK* in HHALI

Figure 10 Database analysis of the biological processes potentially involving *PBK*. (A) Cluster diagram of the top five most enriched terms in the GO enrichment analysis. (B) Cluster diagram of the top five most enriched pathways in the KEGG enrichment analysis. (C) Significantly enriched GO terms according to the differential genes between the LV-NC and LV-*PBK* groups. (D) The top 35 most enriched KEGG pathways of the differential genes between the LV-NC and LV-*PBK* groups. (E) The top 10 most activated states of the biological pathways in the LV-NC and LV-*PBK* groups according to GSEA. FC, fold change; GO, Gene ontology; KEGG, Kyoto Encyclopedia of Genes and Genomes; TNF, tumor necrosis factor; IL-17, interleukin 17; FDR, false discovery rate; GSEA, gene set enrichment analysis; *PBK*, PDZ binding kinase; LV, lentivirus; NC, normal control; BP, biological process; CC, cellular component; MF, molecular function.

PINK1 axis (44). Under normal circumstances, hypoxia and other stress conditions activate the guardian of the genome, *p53*, ultimately resulting in cell cycle arrest (45) to promote the DNA repair mechanism. During this process, *p53* promotes the transcription and activation of downstream target genes that are involved in DNA damage repair. Once the damage is repaired, the cell resumes the cell cycle or restores its normal cellular function (46). If the damage to DNA exceeds a certain threshold or reaches an irreversible state, the cell will be unable to completely restore genomic integrity, which leads to the sustained activation of *p53* (47,48), ultimately resulting in cell senescence, autophagy, and potentially programmed cell death. A study has indicated that there is a complex cascade relationship between *p53* and *SIRT1*, which interact with and mutually influence each other during mitochondrial autophagy and cell apoptosis processes (46). Building upon this, we conducted further research and discovered that *p53* can bind to the promoter region of the *SIRT1* gene, inhibiting the transcription of *SIRT1* and reducing its expression level (49); moreover, *SIRT1* can weaken the activity of the *p53* protein through deacetylation (50). Based on findings reported in the literature, we speculated that when mitochondria undergo oxidative stress due to hypoxia, *PINK1* recognizes unhealthy mitochondria and induces mitophagy, thereby removing mitochondria in an oxidative stress state and reducing oxidative stress. This results in a decreased release of peroxides and superoxides and the reduced recruitment of inflammatory cells (51), ultimately alleviating hypoxia-induced cell apoptosis at the source (52,53). During oxidative stress response, a significant amount of reactive oxygen species is released, recruiting inflammatory cells and resulting in a massive release of local inflammatory factors. Overexpression of PBK activates autophagy, leading to the engulfment of dysfunctional mitochondria, reducing the release of reactive oxygen species, and alleviating local damage. In this study, we used Beas-2b cells and Balb/c mice as experimental materials, established HH cell and animal models, and overexpressed *PBK* in cells and mouse lungs using a lentivirus and adenovirus, respectively. We found that Beas-2b cells and Balb/c mice overexpressing *PBK* were more resistant to HH compared to wild-type cells and mice. Macroscopic observation and HE staining of mouse lungs revealed that *PBK* overexpression significantly alleviated HHALI, reducing pathological manifestations caused by HH in mice, such as pulmonary edema, pulmonary congestion, and inflammatory cell infiltration, and decreasing lung injury scores. In addition, the secretion of inflammatory factors

and oxidative stress markers in mouse lungs was reduced due to *PBK* upregulation, resulting in decreased lung water content and reduced degree of pulmonary edema. In chronic inflammation, the activation of macrophage autophagy can promote macrophage polarization towards the M2 subtype, while conversely, it encourages macrophages to polarize towards the M1 subtype. When a substantial number of macrophages polarize towards the M1 subtype, organs sustain ongoing immune responses, leading to fibrosis in local tissues, which may be associated with chronic damage in local tissues. This study primarily focuses on ALI, with no significant fibrosis or macrophage recruitment observed in HE staining. Therefore, this type of immune response may not function as the cellular mechanism of ALI. The increase in the *Bcl2-BAX* ratio and the decrease in *caspase3* expression in mouse lung tissue, which are related to apoptosis, indicated a certain degree of reduction in apoptosis levels in lung tissue after *PBK* overexpression. The role of *PBK* in promoting cell proliferation and reducing cell apoptosis is mediated by the *p53* protein (54,55). *p53* is considered to be a tumor suppressor, and while *PBK* can activate *SIRT1*, *p53* can inhibit the activation of the *SIRT1* protein to some extent (56,57). Moreover, the overexpression of *PBK* can reduce the level of *p53* protein in mouse lung tissue. Activation of *p53* can block the protective mechanisms against HH-induced ALI, such as reduced apoptosis, decreased secretion of inflammatory factors, decreased oxidative stress levels, and increased mitochondrial autophagy levels caused by *PBK* overexpression. Simultaneous activation of *p53* and *SIRT1* was demonstrated to reverse the aggravated lung injury caused by *p53* activation (58-60). This points to the presence of the upstream and downstream relationship of the *PBK*, *p53*, and the *SIRT1–PINK1* axis. Multiple studies point to the complex cascade relationship between *p53* and *SIRT1* (46,47). In this study, we conducted additional research.

We performed transcriptome sequencing on the successfully constructed *PBK*-overexpressing cell line. First, through differential analysis, we identified the genes that have been reported in other literature and are relevant to our study. GSEA was used to successfully identify enriched pathways with high enrichment scores related to hypoxia, injury, and inflammation, confirming the authenticity and validity of the sequencing data (61). Based on this, we conducted a series of analyses, in which we identified numerous highly scored microRNAs and transcription factors through enrichment analysis. This facilitated the in-depth analysis of the upstream and downstream molecular

2098

Sun et al. The role and mechanism of *PBK* in HHALI

mechanisms of *PBK* that mitigate ALI caused by low pressure and low oxygen via mitochondrial autophagy, as well as the potential alternative pathways. However, substantial follow-up experiments are still needed for verification. Furthermore, we also identified a few immune-related pathways and factors via enrichment. However, this has significant limitations, such as whether *PBK* has an impact on other lung cells and how to specifically activate PBK to protect against HHALI, which is still worth further. This study is entirely animal experiments, and further research should take human specimens from HHALI for further verification. Our team plans to use single-cell transcriptome sequencing at a later stage in research to conduct in-depth analysis of tissue samples, further elucidating their underlying mechanisms.

Conclusions

In this study, we found that *PBK* can serve as a novel potential therapeutic target for HHALI. This therapeutic effect is achieved by inhibiting the activation of p53 protein, thereby promoting the mitochondrial autophagy induced by the *SIRT1-PINK1* axis and thus reducing the secretion of local inflammatory factors and oxidative stress response. Through RNA sequencing, we further discovered that *PBK* may be involved in other signaling pathways in alleviating HHALI, and these should be explored in more detail in subsequent experiments. Further research is needed, as there are still several issues related to this subject which remain unclear, such as how *PBK* regulates *p53* and whether this process involves any protein molecule interactions or changes in protein structure.

Acknowledgments

Footnote

Reporting Checklist: The authors have completed the ARRIVE reporting checklist. Available at https://jtd.amegroups.com/article/view/10.21037/jtd-24-188/rc

Data Sharing Statement: Available at https://jtd.amegroups.com/article/view/10.21037/jtd-24-188/dss

Peer Review File: Available at https://jtd.amegroups.com/article/view/10.21037/jtd-24-188/prf

Conflicts of Interest: All authors have completed the ICMJE uniform disclosure form (available at https://jtd.amegroups.com/article/view/10.21037/jtd-24-188/coif). B.K. serves as the advisory boards for AstraZeneca, BMS, Merck, Roche, and Medtronic. J.Z. is from Xianrenchang (Tianjin) Medical Technology Co., Ltd. The other authors have no conflicts of interest to declare.

Ethical Statement: The authors are accountable for all aspects of the work in ensuring that questions related to the accuracy or integrity of any part of the work are appropriately investigated and resolved. Animal experiments were performed under a project license (No. IRB2023-DW-122) granted by the Animal Welfare and Ethics Committee of Tianjin Medical University General Hospital, in compliance with national guidelines for the care and use of animals.

References

1. Mirrakhimov AE, Strohl KP. High-altitude Pulmonary Hypertension: an Update on Disease Pathogenesis and Management. Open Cardiovasc Med J 2016;10:19-27.
2. Shaw DM, Cabre G, Gant N. Hypoxic Hypoxia and Brain Function in Military Aviation: Basic Physiology and Applied Perspectives. Front Physiol 2021;12:665821.
3. Ahmad Y, Sharma NK, Ahmad MF, et al. Proteomic identification of novel differentiation plasma protein markers in hypobaric hypoxia-induced rat model. PLoS One 2014;9:e98027.
4. Maggiorini M, Bühler B, Walter M, et al. Prevalence of acute mountain sickness in the Swiss Alps. BMJ

1990;301:853-5.

5. Hartmann G, Tschöp M, Fischer R, et al. High altitude increases circulating interleukin-6, interleukin-1 receptor antagonist and C-reactive protein. Cytokine 2000;12:246-52.

6. Maston LD, Jones DT, Giermakowska W, et al. Interleukin-6 trans-signaling contributes to chronic hypoxia-induced pulmonary hypertension. Pulm Circ 2018;8:2045894018780734.

7. Cramer NP, Korotcov A, Bosomtwi A, et al. Neuronal and vascular deficits following chronic adaptation to high altitude. Exp Neurol 2019;311:293-304.

8. Boos CJ, Hodkinson P, Mellor A, et al. The effects of acute hypobaric hypoxia on arterial stiffness and endothelial function and its relationship to changes in pulmonary artery pressure and left ventricular diastolic function. High Alt Med Biol 2012;13:105-11.

9. Montaner JS, Tsang J, Evans KG, et al. Alveolar epithelial damage. A critical difference between high pressure and oleic acid-induced low pressure pulmonary edema. J Clin Invest 1986;77:1786-96.

10. Behinaein P, Hutchings H, Knapp T, et al. The growing impact of air quality on lung-related illness: a narrative review. J Thorac Dis 2023;15:5055-63.

11. Jain K, Prasad D, Singh SB, et al. Hypobaric Hypoxia Imbalances Mitochondrial Dynamics in Rat Brain Hippocampus. Neurol Res Int 2015;2015:742059.

12. Liu L, Feng D, Chen G, et al. Mitochondrial outer-membrane protein FUNDC1 mediates hypoxia-induced mitophagy in mammalian cells. Nat Cell Biol 2012;14:177-85.

13. Siques P, Pena E, Brito J, et al. Oxidative Stress, Kinase Activation, and Inflammatory Pathways Involved in Effects on Smooth Muscle Cells During Pulmonary Artery Hypertension Under Hypobaric Hypoxia Exposure. Front Physiol 2021;12:690341.

14. Peacock AJ. ABC of oxygen: oxygen at high altitude. BMJ 1998;317:1063-6.

15. Gaudet S, Branton D, Lue RA. Characterization of PDZ-binding kinase, a mitotic kinase. Proc Natl Acad Sci U S A 2000;97:5167-72.

16. Herbert KJ, Ashton TM, Prevo R, et al. T-LAK cell-originated protein kinase (TOPK): an emerging target for cancer-specific therapeutics. Cell Death Dis 2018;9:1089.

17. Shinde SR, Gangula NR, Kavela S, et al. TOPK and PTEN participate in CHFR mediated mitotic checkpoint. Cell Signal 2013;25:2511-7.

18. Zhao H, Wang R, Tao Z, et al. Ischemic postconditioning relieves cerebral ischemia and reperfusion injury through activating T-LAK cell-originated protein kinase/protein kinase B pathway in rats. Stroke 2014;45:2417-24.

19. Park JH, Park SA, Lee YJ, et al. PBK attenuates paclitaxel-induced autophagic cell death by suppressing p53 in H460 non-small-cell lung cancer cells. FEBS Open Bio 2020;10:937-50.

20. Gao S, Zhu Y, Li H, et al. Remote ischemic postconditioning protects against renal ischemia/reperfusion injury by activation of T-LAK-cell-originated protein kinase (TOPK)/PTEN/Akt signaling pathway mediated anti-oxidation and anti-inflammation. Int Immunopharmacol 2016;38:395-401.

21. Ayllón V, O'connor R. PBK/TOPK promotes tumour cell proliferation through p38 MAPK activity and regulation of the DNA damage response. Oncogene 2007;26:3451-61.

22. Li H, Qiu D, Yang H, et al. Therapeutic Efficacy of Excretory-Secretory Products of Trichinella spiralis Adult Worms on Sepsis-Induced Acute Lung Injury in a Mouse Model. Front Cell Infect Microbiol 2021;11:653843.

23. Zoulikha M, Xiao Q, Boafo GF, et al. Pulmonary delivery of siRNA against acute lung injury/acute respiratory distress syndrome. Acta Pharm Sin B 2022;12:600-20.

24. Matute-Bello G, Downey G, Moore BB, et al. An official American Thoracic Society workshop report: features and measurements of experimental acute lung injury in animals. Am J Respir Cell Mol Biol 2011;44:725-38.

25. Zhou Y, Li P, Goodwin AJ, et al. Exosomes from endothelial progenitor cells improve outcomes of the lipopolysaccharide-induced acute lung injury. Crit Care 2019;23:44.

26. Acosta-Herrera M, Lorenzo-Diaz F, Pino-Yanes M, et al. Correction: Lung Transcriptomics during Protective Ventilatory Support in Sepsis-Induced Acute Lung Injury. PLoS One 2015;10:e0145696.

27. D'Alessio FR. Mouse Models of Acute Lung Injury and ARDS. Methods Mol Biol 2018;1809:341-50.

28. Millar MW, Fazal F, Rahman A. Therapeutic Targeting of NF-κB in Acute Lung Injury: A Double-Edged Sword. Cells 2022;11:3317.

29. Long ME, Mallampalli RK, Horowitz JC. Pathogenesis of pneumonia and acute lung injury. Clin Sci (Lond) 2022;136:747-69.

30. Tsai SH, Huang PH, Tsai HY, et al. Roles of the hypoximir microRNA-424/322 in acute hypoxia and hypoxia-induced pulmonary vascular leakage. FASEB J 2019;33:12565-75.

31. Jiao Y, Zhang T, Zhang C, et al. Exosomal miR-30d-5p of neutrophils induces M1 macrophage polarization and

2100

Sun et al. The role and mechanism of *PBK* in HHALI

primes macrophage pyroptosis in sepsis-related acute lung injury. Crit Care 2021;25:356.

32. Liu S, Liu Y, Li J, et al. Arsenic Exposure-Induced Acute Kidney Injury by Regulating SIRT1/PINK1/Mitophagy Axis in Mice and in HK-2 Cells. J Agric Food Chem 2023;71:15809-20.

33. Zhao Y, Li HX, Luo Y, et al. Lycopene mitigates DEHP-induced hepatic mitochondrial quality control disorder via regulating SIRT1/PINK1/mitophagy axis and mitochondrial unfolded protein response. Environ Pollut 2022;292:118390.

34. Herrera EA, Farías JG, González-Candia A, et al. Ω3 Supplementation and intermittent hypobaric hypoxia induce cardioprotection enhancing antioxidant mechanisms in adult rats. Mar Drugs 2015;13:838-60.

35. Arya A, Sethy NK, Singh SK, et al. Cerium oxide nanoparticles protect rodent lungs from hypobaric hypoxia-induced oxidative stress and inflammation. Int J Nanomedicine 2013;8:4507-20.

36. Liao Y, Chen Z, Yang Y, et al. Antibiotic intervention exacerbated oxidative stress and inflammatory responses in SD rats under hypobaric hypoxia exposure. Free Radic Biol Med 2023;209:70-83.

37. González-Candia A, Candia AA, Paz A, et al. Cardioprotective Antioxidant and Anti-Inflammatory Mechanisms Induced by Intermittent Hypobaric Hypoxia. Antioxidants (Basel) 2022;11:1043.

38. Lin MT, Beal MF. Mitochondrial dysfunction and oxidative stress in neurodegenerative diseases. Nature 2006;443:787-95.

39. Dionísio PA, Amaral JD, Rodrigues CMP. Oxidative stress and regulated cell death in Parkinson's disease. Ageing Res Rev 2021;67:101263.

40. Zhou J, Li XY, Liu YJ, et al. Full-coverage regulations of autophagy by ROS: from induction to maturation. Autophagy 2022;18:1240-55.

41. Zhao M, Wang Y, Li L, et al. Mitochondrial ROS promote mitochondrial dysfunction and inflammation in ischemic acute kidney injury by disrupting TFAM-mediated mtDNA maintenance. Theranostics 2021;11:1845-63.

42. Tower J. Programmed cell death in aging. Ageing Res Rev 2015;23:90-100.

43. Sauler M, Bazan IS, Lee PJ. Cell Death in the Lung: The Apoptosis-Necroptosis Axis. Annu Rev Physiol 2019;81:375-402.

44. Joel M, Mughal AA, Grieg Z, et al. Targeting PBK/TOPK decreases growth and survival of glioma initiating cells in vitro and attenuates tumor growth in vivo. Mol Cancer 2015;14:121.

45. Levine AJ. p53: 800 million years of evolution and 40 years of discovery. Nat Rev Cancer 2020;20:471-80.

46. Chen X, Zeh HJ, Kang R, et al. Cell death in pancreatic cancer: from pathogenesis to therapy. Nat Rev Gastroenterol Hepatol 2021;18:804-23.

47. Baker SJ, Fearon ER, Nigro JM, et al. Chromosome 17 deletions and p53 gene mutations in colorectal carcinomas. Science 1989;244:217-21.

48. Maor-Nof M, Shipony Z, Lopez-Gonzalez R, et al. p53 is a central regulator driving neurodegeneration caused by C9orf72 poly(PR). Cell 2021;184:689-708.e20.

49. Amano H, Chaudhury A, Rodriguez-Aguayo C, et al. Telomere Dysfunction Induces Sirtuin Repression that Drives Telomere-Dependent Disease. Cell Metab 2019;29:1274-1290.e9.

50. Brooks CL, Gu W. How does SIRT1 affect metabolism, senescence and cancer? Nat Rev Cancer 2009;9:123-8.

51. Liu H, Fisher SA. Hypoxia-inducible transcription factor-1alpha triggers an autocrine survival pathway during embryonic cardiac outflow tract remodeling. Circ Res 2008;102:1331-9.

52. Veith C, Vartürk-Özcan I, Wujak M, et al. SPARC, a Novel Regulator of Vascular Cell Function in Pulmonary Hypertension. Circulation 2022;145:916-33.

53. Du J, Chen Y, Li Q, et al. HIF-1α deletion partially rescues defects of hematopoietic stem cell quiescence caused by Cited2 deficiency. Blood 2012;119:2789-98.

54. Hu F, Gartenhaus RB, Eichberg D, et al. PBK/TOPK interacts with the DBD domain of tumor suppressor p53 and modulates expression of transcriptional targets including p21. Oncogene 2010;29:5464-74.

55. Lei B, Liu S, Qi W, et al. PBK/TOPK expression in non-small-cell lung cancer: its correlation and prognostic significance with Ki67 and p53 expression. Histopathology 2013;63:696-703.

56. Sasca D, Hähnel PS, Szybinski J, et al. SIRT1 prevents genotoxic stress-induced p53 activation in acute myeloid leukemia. Blood 2014;124:121-33.

57. Leblond A, Pezet S, Cauvet A, et al. Implication of the deacetylase sirtuin-1 on synovial angiogenesis and persistence of experimental arthritis. Ann Rheum Dis 2020;79:891-900.

58. Xu Y, Wan W. Acetylation in the regulation of autophagy. Autophagy 2023;19:379-87.

59. Chen WY, Wang DH, Yen RC, et al. Tumor suppressor HIC1 directly regulates SIRT1 to modulate p53-dependent DNA-damage responses. Cell 2005;123:437-

48.

60. Vakhrusheva O, Smolka C, Gajawada P, et al. Sirt7 increases stress resistance of cardiomyocytes and prevents apoptosis and inflammatory cardiomyopathy in mice. Circ Res 2008;102:703-10.

61. Wen H, Chen Z, Li M, et al. An Integrative Pan-Cancer Analysis of PBK in Human Tumors. Front Mol Biosci 2021;8:755911.
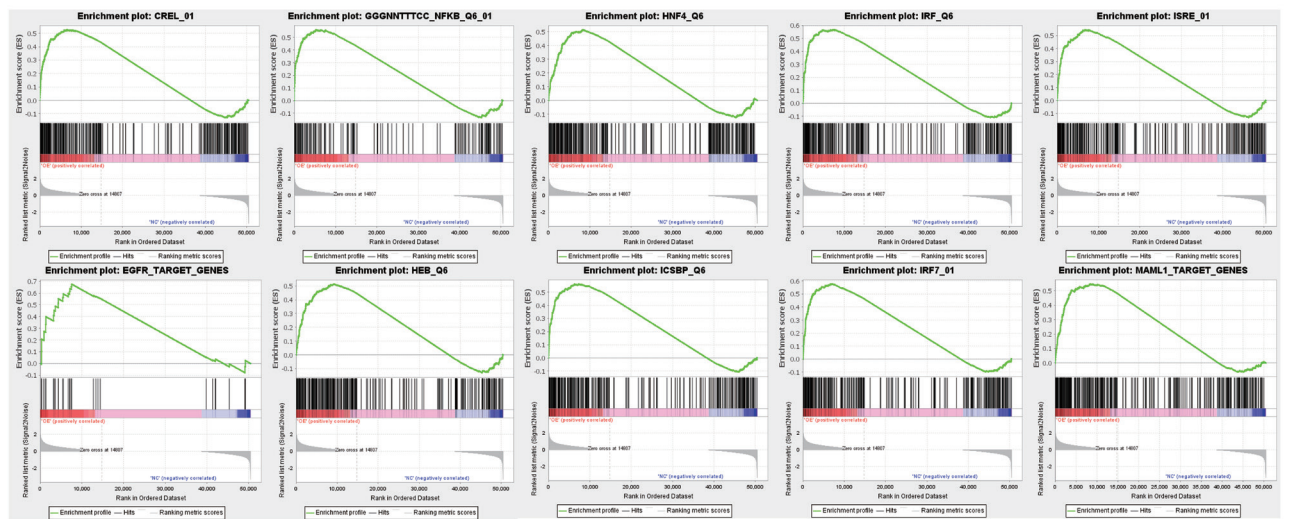
A
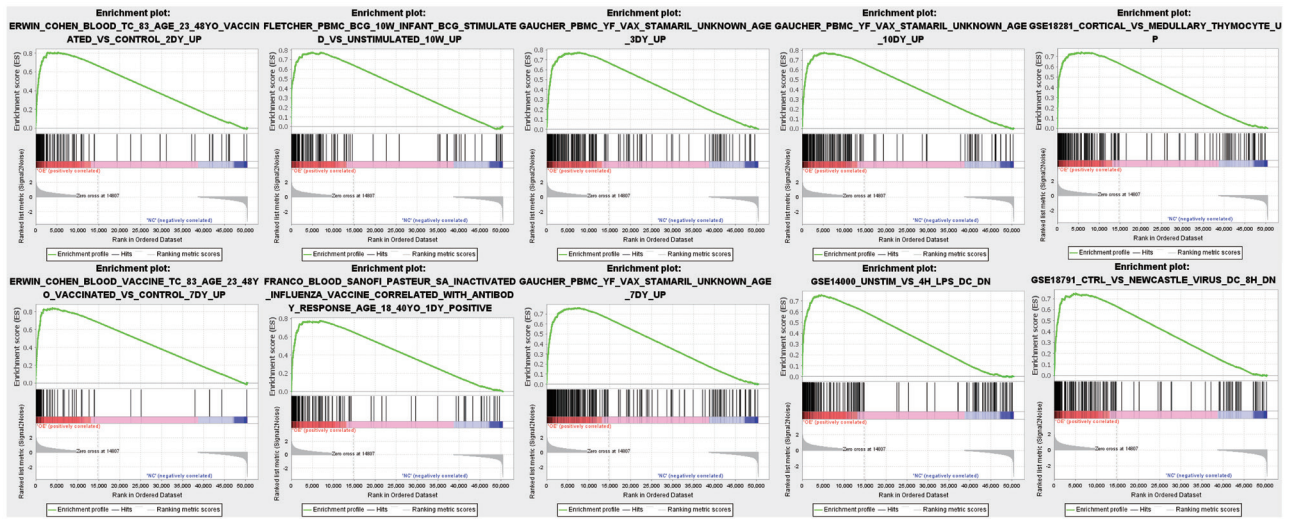
B

Figure S1 The relevant signaling pathways potentially involving *PBK*. (A,B) GSEA enrichment analysis showing the top most 10 activated states of the biological pathways in the LV-NC and LV-*PBK* groups. GSEA, gene set enrichment analysis; *PBK*, PDZ binding kinase; LV, lentivirus; NC, normal control.